Influence Analysis of Damp Defect of Composite Insulated Zinc Oxide Arrester Based on Finite Element Calculation

Wenyan Li, Jiangming Liu, Lintao Sun, Changbiao Liu, Yunfei Ai, Zhi Wang, Jie Zhou, and Ke Ye

Abstract Composite insulated zinc oxide arrester is important electrical equipment in power systems, and is prone to insulation failure during operation. For a case of abnormal leakage current and heat generation of zinc oxide arrester, the cause of the abnormality was identified as internal dampness through testing and disintegration analysis. The finite element analysis method was used to study the effects of zinc oxide valve plate moisture, insulating sheath moisture and insulating sheath cracking on the voltage distribution of arrester. The results show that when the resistivity of the arrester varistors and sheaths drops to a certain extent, it will lead to a significant change in the voltage distribution on the varistors, and the overall change trend is that the voltage of the varistors around the object is reduced, and the voltage of the other varistors is raised. It plays a certain a certain reference role in the analysis and disposal of the insulation moisture abnormality of the composite insulated zinc oxide arrester.

Keywords Arrester · Dampness · Defect · Finite element calculation

1 Introduction

Zinc oxide arrester is an overvoltage limiting device with excellent nonlinear voltammetric characteristics, and its operating performance plays a major role in the safe operation of power equipment [1]. Statistical analysis data show that internal moisture, impact damage, pollution damage, improper use are the main reasons for the failure of the arrester. Among them, the proportion of internal moisture caused by seal failure and external force failure can reach 85.6% of the statistics of the number of arrester failure causes [2].

W. Li (✉) · J. Liu · L. Sun · C. Liu · Y. Ai · Z. Wang · J. Zhou · K. Ye
State Grid Zhejiang Electric Power Co., Ltd., Ultra-High Voltage Branch Company, Hangzhou 310000, China
e-mail: 526152295@qq.com

X. Dong and L. Cai (eds.), *The Proceedings of 2023 4th International Symposium on Insulation and Discharge Computation for Power Equipment (IDCOMPU2023)*, Lecture Notes in Electrical Engineering 1102, https://doi.org/10.1007/978-981-99-7405-4_38

Aiming at the moisture phenomenon of porcelain sleeve structure arrester, it is pointed out that the resistance value of the resistance valve plate decreases when the arrester is wet, the leakage current flowing through the arrester increases, the dielectric loss increases, and there is local overheating in the damp part [3]. A simulation test was carried out on the internal and external temperature distribution characteristics and electrical parameters of a single section of the arrester under the condition of moisture with 1000 kV zinc oxide arrester as the research object, and it was pointed out that the optical fiber temperature measurement method and infrared temperature measurement method could effectively determine the internal moisture defects of the zinc oxide arrester, while the electrical parameters were not sensitive enough for the moisture reaction of the single section of the UHV zinc oxide arrester [4]. Scholars at home and abroad use simulation tests, live detection and finite element simulation analysis to characterize the internal temperature, voltage and electric field distribution of the arrester under abnormal conditions such as internal moisture and external surface pollution [5–14]. The optical fiber-current method is used to verify the correctness of the finite element analysis calculation method and results in the calculation of arrester voltage and electric field distribution [15]. However, there is less research on the insulation failure of single-section composite insulated zinc oxide arrester partial valve plate and sheath.

Aiming at the influence of local moisture in composite insulated zinc oxide arrester, the author uses the finite element method to study and analyze the influence of moisture exposure and sheath cracking on the overall voltage distribution of the arrester valve by a case of abnormal leakage current of 220 kV composite insulated zinc oxide arrester.

2 Device Abnormality

The live detection of a 500 kV substation found that the leakage current of phase B and C of a 220 kV line zinc oxide arrester increased significantly, and the heating was abnormal. The arrester model is YH10W-216/562, which is made of two stages in series, and the main components include flange, zinc oxide valve plate, zinc oxide valve fixture, insulating cylinder, silicone rubber umbrella skirt. Each section of the arrester contains 30 resistive valve plates, each 15 resistive valve plates are fixed with a insulating sheath, and the zinc oxide valve plate and the sheath are filled with micro-positive pressure nitrogen. In order to adjust the height of the zinc oxide valve plate so that it fits with the outer insulation, metal gaskets are placed between the partial zinc oxide valve plates. The structure of the device is shown in Fig. 1.

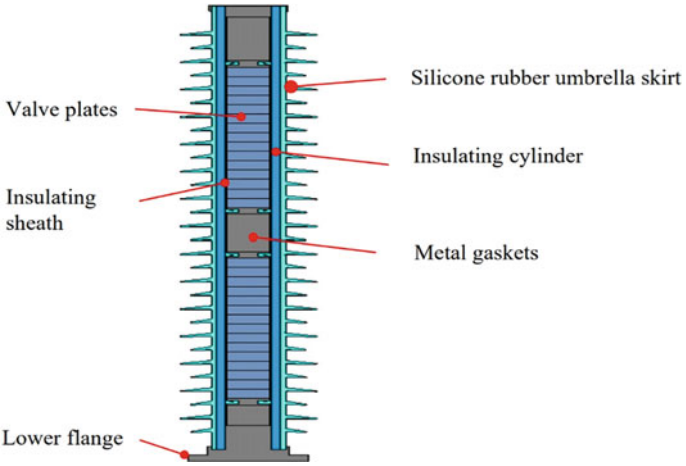

Fig. 1 Structural diagram of polymeric insulated zinc oxide arrester

2.1 Leakage Current Detection at Continuous Operating Voltage

The leakage current detection of the zinc oxide arrester shows that the full current and resistive current components of the B-phase and C-phase arresters are significantly increased, and the leakage current live detection data are shown in Table 1.

As can be seen from Table 1:

(1) Compared with the detection data in 2019 and 2020, the impedance angle of the three-phase arrester detection data in 2021 is reduced by 2–5 degrees, and the full current of the B-phase and C-phase arresters and the resistive current of the three-phase arrester increased significantly, of which the full current of the B-phase arrester increases by 0.03 mA and the resistive current increased by 0.032 mA compared with 2020, with growth rates of 8.0 and 94.1% respectively;

Table 1 Leakage current of polymeric insulated zinc oxide arrester

Phase	φ/°	I_X/mA	Ir/mA	Irp/mA	Ir1p/mA	Ir3p/mA	Year of detection
A	**86.88**	**0.442**	**0.025**	0.035	0.034	0.007	2019
	87.11	**0.441**	**0.024**	0.032	0.031	0.007	2020
	84.42	**0.447**	**0.045**	0.069	0.061	0.007	2021
B	**84.10**	**0.377**	**0.039**	0.059	0.055	0.007	2019
	84.91	**0.375**	**0.034**	0.049	0.047	0.005	2020
	80.72	**0.405**	**0.066**	0.097	0.092	0.007	2021
C	**86.81**	**0.398**	**0.023**	0.033	0.031	0.007	2019
	86.97	**0.399**	**0.023**	0.033	0.029	0.005	2020

The full current of C-phase arresters increased by 0.17 mA and resistive current increased by 0.028 mA compared with 2020, with growth rates of 4.3 and 47.8%, respectively.

(2) In the A-phase and C-phase angle test, automatic edge replenishment technology is used to counteract the interference effect of stray capacitance between phases on the linear arrester resistance current sensing data. That is, the B-phase detection data in the automatic edge complement mode is the real value, while the A-phase and C-phase resistive current detection data are related to the compensation angle, if one phase equipment is abnormal, the other phase equipment data will be affected. According to the full current detected in 2021 and the compensation angle under normal conditions in 2019, the resistance current data of the A-phase and C-phase arresters are calculated to be 0.023 and 0.059 mA, respectively. That is, the detection data of A-phase arrester in 2021 had no significant change compared with previous years, and the C-phase arrester resistive current increased by 0.036 mA, with a growth rate of 156.5%.

2.2 Infrared Imaging Temperature Measurement

The infrared imaging spectrum of the arrester is shown in Fig. 2. Comparing the temperature of the upper section of the three-phase arrester, it can be found that the maximum surface temperature of the B-phase and C-phase arresters is 22.4 and 20.2 °C, respectively, which are greater than 3.8 and 1.6 K of the A-phase arrester, which exceeds the requirements of DL/T664-2008 "Infrared Diagnostic Application Specification for Live Equipment" for the temperature difference of the arrester is not more than 1 K, which is a serious defect.

3 Disintegration Examination

The B-phase arrester was disassembled, and it was found that the upper section valve plate group had high resistance during the disassembly process, and the insulation sheath cracked and deformed many times. The upper section of the A phase with normal test data was disassembled, and it was found that the valve plate group was taken out smoothly, and the outer insulation sheath of the valve plate group was intact and there was no abnormality. The appearance of the upper insulating sheath of the A-phase and B-phase arresters is shown in Fig. 3.

The two valve groups taken out of the upper section of the B-phase arrester have different degrees of insulation sheath cracking, in which 7 zinc oxide valve plates are exposed at the top crack of the insulation sheath of the upper valve plate group, and some of the exposed surfaces of the valve discs together with the surface of the top metal electrode have obvious ablation marks, as shown in Fig. 4.

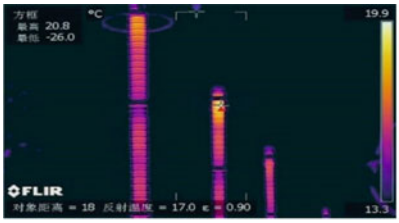

(a) Three-phase arrester as a whole

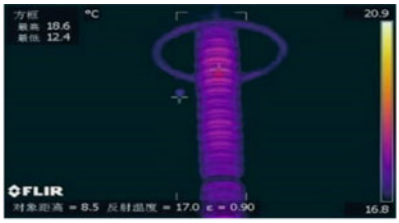

(b) A-phase arrester section above

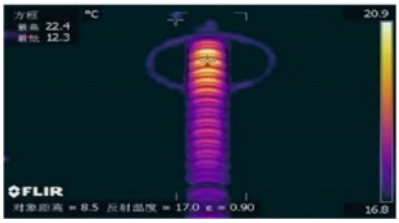

(c) B-phase arrester section above

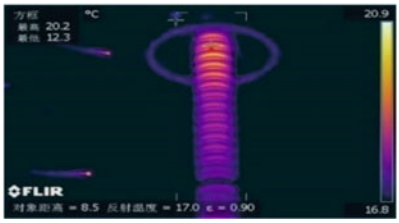

(d) C-phase arrester section above

Fig. 2 Infrared imaging temperature measurement picture

(a) A-phase arrester section above

(b) B-phase arrester section above

Fig. 3 The appearance of insulated sheath

The insulation resistance test was carried out on 4 zinc oxide valve plates with obvious ablation marks on the exposed surface of the valve plate, and the insulation resistance data was obtained as shown in Table 2.

As can be seen from Table 2, the insulation resistance test results carried out immediately after the disintegration of the four resistance valve plates show that the insulation resistance of the valve plate is 2–4 MΩ. After wiping the surface of the

(a) (b)

Fig. 4 The cracked sheath and discharged trace

Table 2 Insulation resistance of zinc oxide varistor

Valve plate serial number	After disintegration/MΩ	After the surface is cleaned/MΩ	After drying treatment/MΩ
1	2.6	560	1640
2	2.91	680	1440
3	2.65	1860	2210
4	3.24	2160	2240

valve plate with alcohol, the insulation resistance increased significantly, and after further drying in the oven, the insulation resistance of the four valve plates reached more than 1500 MΩ. The above indicates that the resistive valve has significant insulating moisture.

Based on the resistive current test, infrared imaging temperature measurement and disintegration of the arrester, it is judged that the abnormal development process of the arrester is that the internal insulation of the valve plate and sheath is moisture, and the insulation resistance decreases. The heating effect caused by the increase of resistive current causes the sheath to crack, the internal electric field is distorted, and the side of the sheath and valve plate is partially discharged.

4 Arrester Voltage and Electric Field Analysis Based on Finite Element Method

In order to study the influence of moisture inside the arrester, the finite element method is used to study the voltage distribution of the arrester under the condition of arrester valve plate, sheath moisture and sheath cracking.

4.1 Finite Element Analysis Method and Simulation Model

The surrounding area of the arrester can be approximated as a fixed-frequency time harmonic field with the high-voltage end as the source. The power frequency voltage of China's power system is 50 Hz, and the wavelength is about 6000 km, which is far greater than the structural height of the arrester, so the coupling between the electric field and the magnetic field is very weak and can be regarded as a quasi-static field. Maxwell's equation under quasi-static conditions is used to establish the computational model of electromagnetic phenomena, and the medium containing poor conductors satisfies the following Poisson equation and boundary conditions.

$$\begin{cases} -(\sigma + \mathrm{j}\omega\varepsilon)\nabla^2\varphi = 0, \quad \text{Within the boundary } \Omega \\ \varphi = \mathrm{u}, \quad \text{Within the boundary } \Gamma_1 \\ \dfrac{\partial\varphi}{\partial n} = \Psi \quad \text{Within the boundary } \Gamma_2 \\ \oint_{\Gamma 0}(\sigma + \mathrm{j}\omega\varepsilon)\dfrac{\partial\varphi}{\partial n}d\Gamma = Q_C, \varphi = \varphi_c, \quad \text{Within the boundary } \Gamma_2 \end{cases}$$

Wherein, Ω is the solution field of potential, which is enclosed by the first class boundary Γ_1 and the second class boundary Γ_2, and contains a suspended conductor Γ_0 in the field; u is the potential function given on Γ_1, is the function given on Γ_2, is the net charge on the potential suspension conductor Γ_0, δ, ε, ω are the conductivity, relative permittivity and power frequency of the material, respectively, and the conductivity and relative permittivity of the material can be regarded as constants at power frequency. φ_C is the potential values to be sought.

Ignoring the upper leads, equalizing rings and other structures, the YH10W-216/562 composite insulated zinc oxide arrester was used as the simulation model, and a three-dimensional axisymmetric model was established in ANSYS electromagnetic field analysis software. Set the two-dimensional element type to plane 230, the three-dimensional element type to solid 231, and the permittivity and resistivity parameters of the conductor and dielectric under good insulation are shown in Table 3. Load a power frequency voltage with the amplitude of the peak phase voltage of the 220 kV line operation at the top electrode of the arrester; A 0 potential is loaded at the bottom electrode and the outer air boundary and solved using the ICCG solver. Extract the

Table 3 Material parameters

Material properties	Gas	Silicone rubber	Insulating cylinder	Insulating sheath	Valve plate	Metal electrode
Dielectric constant	1	4.75	3	3.5	750	60,000
Resistivity/ $\Omega\ m^{-1}$	1e8	1e12	5e11	1e12	1e12	–

potential at the upper and lower points of each valve plate, and calculate the voltage borne by the valve plate (Table 3).

4.2 The Valve Plate is Affected by the Degree of Moisture on the Voltage Distribution of the Arrester

When the resistivity of the 1–15 valve plates of the upper section arrester from top to bottom is set Separately to 1e12, 1e6, 1e5 and 1e4 $\Omega\ m^{-1}$, the voltage distribution of the arrester is shown in Fig. 5.

It can be seen from Fig. 5 that due to the comprehensive factors of its own capacitance and stray capacitance, the potential distribution of the arrester resistance valve plate is uneven. In the absence of pressure equalization measures, the potential distribution is characterized by high voltage sharing of the upper valve plate and low voltage sharing of the lower valve plate, which makes the charge rate of some valve plates high. When the resistivity of the 1–15th valve plate changes in the range of 1e6–1e12 $\Omega\ m^{-1}$, the overall voltage distribution of the arrester does not change significantly, but when the resistivity of the 1–15th valve plate drops to 1e4 $\Omega\ m^{-1}$,

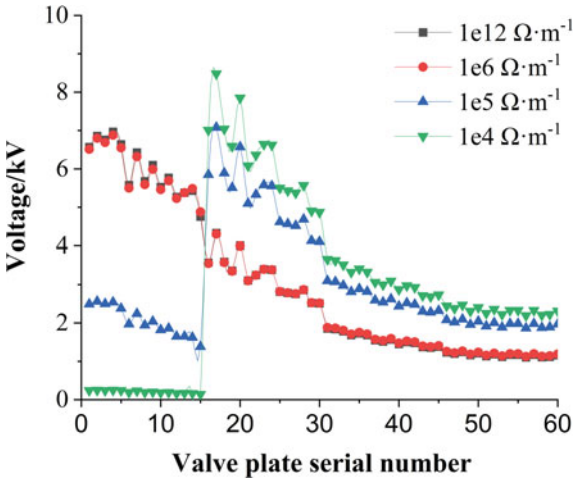

Fig. 5 The voltage distribution under different electrical resistivity of zinc oxide varistor

the bearing voltage of the single valve plate with the decrease in resistivity decreases significantly, from a few thousand volts to hundreds of volts, while the voltage of other valve plates rises significantly, resulting in uneven voltage distribution.

4.3 Effect of Sheath Cracking Angle on Arrester Voltage Distribution.

Under the condition that the cracking angles of the outer sheath of the 1–15 valve disc from top to bottom are 15°, 30° and 45°, the voltage distribution of the arrester valve plate is shown in Fig. 6.

It can be seen from Fig. 6 that in the absence of moisture in the insulation layer, the cracking of the sheath has a great effect on the voltage of the lightning arrester valve near it, and the voltage change of the lightning arrester valve piece far from the cracking position of the sheath is not obvious. Compared with the case that the sheath is not cracked, after the sheath is cracked, the bearing voltage of the top resistive valve plate dominated by the 1–6 pieces decreases, and the withstand voltage of the middle and lower resistive valve plates increases slightly, that is, the voltage distribution of the upper arrester valve plate tends to be uniform.

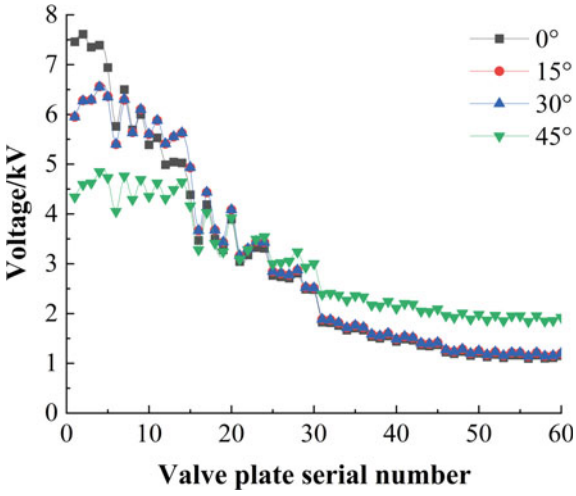

Fig. 6 The voltage distribution under different cracked angles of insulated sheath

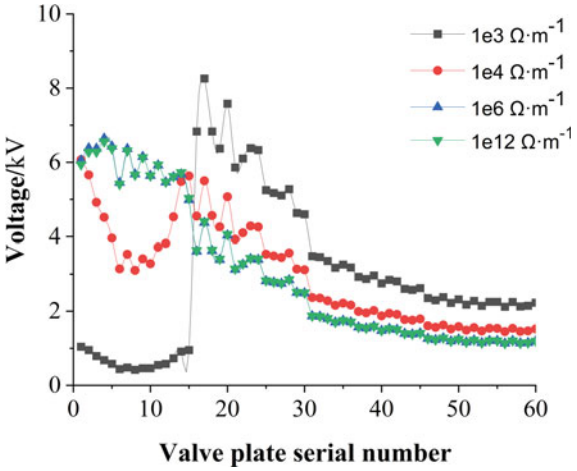

Fig. 7 The voltage distribution under different electrical resistivity of insulated sheath

4.4 The Influence of Moisture Degree of the Sheath on the Voltage and Electric Field Distribution of the Arrester

The sheath cracking angle is set to 45°, and the sheath resistivity changes in the range of 1e3–1e12 Ω m^{-1}, and the voltage distribution on the arrester valve plate under the condition of simulating the sheath under moisture is shown in Fig. 7.

It can be seen from Fig. 7 that when the sheath resistivity is in the range of 1e3–1e12 Ω m^{-1}, the arrester voltage distribution curve is highly coincident, that is, the decrease in sheath insulation resistance in this range has little effect on the voltage distribution of the valve piece. When the sheath resistivity drops to 1e4 Ω m^{-1}, the valve plate voltage distribution changes significantly. This change is mainly manifested as the voltage bearing of the valve plate adjacent to the position of the moisture-bearing sheath drops, the voltage of other valve plates rises, and the bearing voltage of individual valve plates becomes about 2 times that of normal.

4.5 Analysis of the Influence of Insulation Moisture on Composite Insulation Arrester

The full current of metal zinc oxide arrester mainly includes the current through the valve plate, the current through the fixed valve plate insulation material and the current through the umbrella skirt. Under normal operating conditions, the full current is mainly capacitive current, and the resistive current only accounts for 10–20%.

From the calculation results of finite element analysis, it can be seen that the resistivity of any material in the arrester valve plate and sheath caused by insulation

moisture will lead to a significant change in the voltage distribution on the valve plate, and the overall change trend is that the voltage of the valve plate around the object with low resistivity decreases, while the voltage of other valves increases, mainly because the insulation moisture causes the impedance change of the valve plate, sheath and other insulation materials, so that the voltage distribution changes.

5 Concluding Remarks

Combining the abnormal characterization of arresters, equipment disintegration and ANSYS finite element analysis, the following conclusions are drawn:

(1) The internal insulation of the arrester will increase the resistive current under the operating voltage, and the heating effect is obvious. Therefore, resistive current testing, infrared imaging temperature measurement and other tests can be carried out in strict accordance with the equipment detection cycle, which can effectively find the internal moisture defects of the arrester.
(2) When the resistivity of the arrester valve plate and sheath drops to a certain extent, it will cause the voltage distribution on the valve plate to change significantly. The overall change trend is that the voltage around the resistivity falling object bears the voltage; The voltage of other valve plates rises, and the charge rate increases.

References

1. Qiao X, Zhang Z, Sundararajan R et al (2021) The failure arc paths of the novel device combining an arrester and an insulator under different pollution levels. Int J Electr Power Energy Syst 125:106549
2. Lyu H (2021) Key technologies and applications of power transmission and transformation equipment lightning arrester. China Electric Power Press, Beijing (in Chinese)
3. Liu W, Xiao J, Jin S et al (2022) Analysison damp defect of 500 kV zinc oxide arrester based on field-circuit coupling. Insul Surge Arresters 1:118–125 (in Chinese)
4. Shi Z, Duan T, Li Z et al (2020) Experimental analysis on dampness defect of UHV zinc oxide arrester. Insul Surge Arrest 6:117–121 (in Chinese)
5. 3D potential distribution calculation and design of grading rings for post-type ZnO surge arrester for 1000 kV substation. In: Proceedings of the Chinese Society for electric engineering (2007), vol 27 (in Chinese)
6. Wang X (2015) MOA failure diagnosis and practical case analysis based on live detection technology. Insul Surge Arresters 3:69–73 (in Chinese)
7. Yan Y, Huang W, Jiang J et al (2011) Principle and instrument comparison of arrester live line test and analysis on the flaw in field. Insul Surge Arresters 2011(2):57–62 (in Chinese)
8. Zhang J (2015) Application of infrared temperature measurement technology to live detection of zinc oxide arrester. High Volt Appar 51(6):200–204 (in Chinese)
9. Zeng G, Li G, Zhang C et al (2020) Simulation analysis of temperature rise distribution characteristics of damp arrester. Hubei Electric Power 44(5):34–41 (in Chinese)

10. Zhang B,Li G, Zhang C et al (2011) Internal temperature rise of MOA under pollution condition. High Volt Eng 37(08):2065–2072 (in Chinese)
11. Liu J (2021) Simulation of radial electric field and voltage distribution of 500 kV MOA under different pollution conditions. Insul Surge Arrest 1 (in Chinese)
12. Wang Q, Gu C, Shi Fet al (2014) Analysis of surge arresters cavity humid caused flashover accident. Appl Mechan Mater 543–547:717–7221
13. Chrzan KL (2010) Failures and destructions of surge arresters. Energetyka 5:281–284
14. Singh RP, Singh TVP (2002) Influence of pollution on the performance of metal oxide surge arresters. In: IEEE Canadian conference on electrical and computer engineering (CCECE 2002), vol 1, pp 224–229
15. Sun H, Li X (2010) Finite element calculation and experiment of potential distribution for a 500 kV Porcelain zinc oxide arrester. High Volt Apparat 3 (in Chinese)